Small Molecule Peptidomimetics Containing a Novel Phosphotyrosine Bioisostere Inhibit Protein Tyrosine Phosphatase 1B and Augment Insulin Action‡

John E. Bleasdale,*,§ Derek Ogg,|| Barbara J. Palazuk,§ Cynthia S. Jacob,§ Michael L. Swanson,§ Xin-Yuan Wang,§ David P. Thompson,§ Robert A. Conradi,§ W. Rodney Mathews,§ Alice L. Laborde,§ Christopher W. Stuchly,§ Anna Heijbel,|| Katrin Bergdahl,|| Carol A. Bannow,§ Clark W. Smith,§ Carina Svensson,|| Charlotta Liljebris,⊥ Heinrich J. Schostarez,§ Paul D. May,§ F. Craig Stevens,§ and Scott D. Larsen§

Research and Development, Pharmacia Corporation, Kalamazoo, Michigan 49007, and Research and Development, Pharmacia Corporation, Stockholm and Uppsala, Sweden

Received December 18, 2000; Revised Manuscript Received March 16, 2001

ABSTRACT: Protein tyrosine phosphatase 1B (PTP1B) attenuates insulin signaling by catalyzing dephosphorylation of insulin receptors (IR) and is an attractive target of potential new drugs for treating the insulin resistance that is central to type II diabetes. Several analogues of cholecystokinin$^{26-33}$ (CCK-8) were found to be surprisingly potent inhibitors of PTP1B, and a common N-terminal tripeptide, *N*-acetyl-Asp-Tyr(SO_3H)-Nle-, was shown to be necessary and sufficient for inhibition. This tripeptide was modified to reduce size and peptide character, and to replace the metabolically unstable sulfotyrosyl group. This led to the discovery of a novel phosphotyrosine bioisostere, 2-carboxymethoxybenzoic acid, and to analogues that were >100-fold more potent than the CCK-8 analogues and >10-fold selective for PTP1B over two other PTP enzymes (LAR and SHP-2), a dual specificity phosphatase (cdc25b), and a serine/threonine phosphatase (calcineurin). These inhibitors disrupted the binding of PTP1B to activated IR in vitro and prevented the loss of tyrosine kinase (IRTK) activity that accompanied PTP1B-catalyzed dephosphorylation of IR. Introduction of these poorly cell permeant inhibitors into insulin-treated cells by microinjection (oocytes) or by esterification to more lipophilic proinhibitors (3T3-L1 adipocytes and L6 myocytes) resulted in increased potency, but not efficacy, of insulin. In some instances, PTP1B inhibitors were insulin-mimetic, suggesting that in unstimulated cells PTP1B may suppress basal IRTK activity. X-ray crystallography of PTP1B−inhibitor complexes revealed that binding of an inhibitor incorporating phenyl-*O*-malonic acid as a phosphotyrosine bioisostere occurred with the mobile WPD loop in the open conformation, while a closely related inhibitor with a 2-carboxymethoxybenzoic acid bioisostere bound with the WPD loop closed, perhaps accounting for its superior potency. These CCK-derived peptidomimetic inhibitors of PTP1B represent a novel template for further development of potent, selective inhibitors, and their cell activity further justifies the selection of PTP1B as a therapeutic target.

In type II diabetes, tissues develop resistance to the actions of insulin even though, in most instances, the insulin receptors in those tissues are structurally normal and are in near-normal abundance (*1*). One strategy to combat this insulin resistance therapeutically may be to maintain insulin receptors (IRs)[1] in the active tyrosine-phosphorylated form by inhibiting enzymes that catalyze IR dephosphorylation. There is evidence that protein tyrosine phosphatase 1B (PTP1B) catalyzes IR dephosphorylation and is involved physiologically and pathologically in terminating insulin signaling. This evidence includes descriptions of both in vitro (*2*, *3*) and in vivo (*4*) interactions between PTP1B and the IR. Purified PTP1B dephosphorylates the IR, apparently in the sequence observed in vivo, and dephosphorylation results in loss of IR tyrosine kinase activity (*5*). Intracellular delivery of neutralizing antibodies against PTP1B was found to augment IR and insulin receptor substrate (IRS)-1 phosphorylation (*6*), while conversely, overexpression of PTP1B in transfected cells inhibited IR and IRS-1 phosphorylation (*7*). Furthermore, PTP1B activity is increased in some tissues of obese insulin resistant patients (*8*) and is reduced in parallel with the increased insulin sensitivity that accompanies weight loss (*8*, *9*). Experimentally induced insulin resistance in a variety of cell models is accompanied by an increase in PTP1B activity (*10*, *11*). In addition, correction of glucose-induced insulin resistance in Rat1 fibroblasts with a thiazolidinedione insulin sensitizer also corrects the elevation of PTP1B activity in the insulin resistant cells (*11*). Recently,

‡ Atomic coordinates for structures of PTP1B−inhibitor complexes determined using X-ray crystallography have been deposited with the Protein Data Bank as entries 1G7F and 1G7G.

* To whom correspondence should be addressed: Cell & Molecular Biology, 7252-267-303, Pharmacia Corp., 301 Henrietta St., Kalamazoo, MI 49007. Telephone: (616) 833-9559. Fax: (616) 833-4255. E-mail: John.E.Bleasdale@am.pnu.com.

§ Pharmacia Corp., Kalamazoo, MI.

|| Research and Development, Pharmacia Corp., Stockholm, Sweden.

⊥ Research and Development, Pharmacia Corp., Uppsala, Sweden.

[1] Abbreviations: CCK-8, C-terminal octapeptide of cholecystokinin; GVBD, germinal vesicle breakdown; HGI, high glucose with insulin; IR, insulin receptor; IRS-1 and -2, insulin receptor substrate-1 and -2, respectively; IRTK, insulin receptor tyrosine kinase; pNPP, *p*-nitrophenyl phosphate; PTP1B, protein tyrosine phosphatase 1B; pTyr, phosphotyrosine; RT-PCR, reverse transcription-polymerase chain reaction; SPA, scintillation proximity assay.

10.1021/bi002865v CCC: $20.00
Published on Web 04/21/2001

it was reported that PTP1B null mice have increased insulin sensitivity and decreased susceptibility to diet-induced obesity (*12*).

PTP1B, therefore, is an attractive therapeutic target, and several investigators have described small molecule inhibitors (*13*−*20*). In general, those inhibitors either are not very potent or contain peptide bonds or other groups that make them pharmacokinetically unattractive as leads for a therapeutic agent. Furthermore, some of those inhibitors contain functionalities capable of reacting with the catalytically essential Cys^{215} of PTP1B and so may be irreversible inhibitors. The purpose of this investigation was to exploit our serendipitous observation that peptide analogues of cholecystokinin (CCK) are surprisingly potent inhibitors of PTP1B in vitro. We report molecular modifications of the original CCK analogue that reduced peptidic characteristics and introduced a novel phosphotyrosine bioisostere (*21*)[2] while increasing potency >100-fold. These small molecules have been used to test the hypothesis that inhibition of PTP1B will augment insulin action. X-ray crystallography of two PTP1B−inhibitor complexes revealed two distinct binding modes and indicated further chemical modifications that might improve potency and selectivity.

MATERIALS AND METHODS

Recombinant PTP Enzymes. A C-terminal truncated, soluble form of human PTP1B (amino acids 1−321) was generated from human placental RNA by RT-PCR and cloned into pET15 (Novagen) at *Kpn*I and *Bam*HI to generate pMB471. This construct was employed to produce PTP1B to screen for inhibitors, for kinetic analyses, and for oocyte microinjections. A similar construct with the addition of an N-terminal His_6 tag and enterokinase cleavage site (pMB428) was also generated. For assays of PTP1B binding to the IR, PTP1B was rendered catalytically inactive by mutating Cys^{215} to Ser^{215} (*22*). A site-directed mutation (C215S) was introduced between *Xho*I and *Bam*HI by PCR using pMB428 as a template to generate pMB476 which was expressed in *Escherichia coli* BL21 grown in sulfur-free M9 minimum medium supplemented with $^{35}SO_4^{2-}$. A fourth construct comprising amino acids 1−298 without the His_6 tag or enterokinase cleavage site (pMB562) was employed for X-ray crystallography. Standard purification procedures of Ni chelation chromatography, ion exchange, and size exclusion chromatography were performed to obtain proteins that were >95% pure and catalytically active. A C-terminally truncated, soluble form of rat PTP1 (amino acids 1−322) was obtained from J. E. Dixon (The University of Michigan, Ann Arbor, MI) as was a GST fusion protein containing the two tyrosine phosphatase domains of human LAR and a GST−SHP-2 fusion protein.

Assays for PTP Activity. PTP1B activity was routinely measured as the rate of hydrolysis of *p*-nitrophenyl phosphate (pNPP) in a 96-well microtiter plate format. Standard assays were conducted at room temperature in a total volume of 0.2 mL that contained Hepes buffer (50 mM, pH 7.2), NaCl (50 mM), EDTA (1 mM), DTT (1 mM), bovine serum albumin (1 mg/mL), pNPP (at various concentrations, $K_m = 1.4 \pm 0.03$ mM), and PTP1B (35 ng/mL). Inhibitors were added in DMSO at 100 times the final concentration. For determinations of inhibitor kinetics, plots of *V* versus *S* at various concentrations of inhibitor were generated and K_i values were computed using the direct linear method of Cornish-Bowden (Enzpack3 software, Biosoft, Cambridge, U.K.). In some experiments, PTP1B activity was measured as the rate of inorganic phosphate released upon hydrolysis of the IR phosphopeptide, TRDIpYETDpYpYRK, using a malachite green method (*23*).

Activities of LAR and SHP-2 were measured as described above except that the Hepes buffer (50 mM) was at pH 6.8 and 7.0, respectively, and each enzyme was added at a concentration of 10 μg/mL. Activity of cdc25b was also measured similarly except the assay buffer was Tris-HCl (50 mM, pH 8.0), and the cdc25b−GST fusion protein was added at a concentration of 20 μg/mL. Activity of calcineurin (from Sigma Chemical Co.) was assayed using 4-methylumbelliferyl phosphate (0.8 mM) as a substrate in an assay mixture that contained Tris-HCl buffer (40 mM, pH 8.6), NaCl (100 mM), $CaCl_2$ (0.5 mM), DTT (0.5 mM), bovine serum albumin (0.1 mg/mL), calmodulin (50 nM), and calcineurin (25 nM). Fluorescence at 450 nm was monitored with excitation at 400 nm.

Cell Measurements. 3T3-L1 cells were maintained in 35 mm plastic culture dishes and differentiated to the adipocyte phenotype using standard procedures as described elsewhere (*24*). Insulin resistance in 3T3-L1 adipocytes was induced by incubating the cells in Dulbecco's modified Eagle's medium supplemented with heat-inactivated fetal bovine serum (10%, v/v), glucose (25 mM), and bovine insulin (100 nM). L6 cells were kindly provided by A. Klip (University of Toronto, Toronto, ON) and were maintained in 35 mm plastic culture dishes and differentiated to myotubes as described by Klip and co-workers (*25*). Effects of PTP1B inhibitors on glucose transport were assessed by measuring the rate of uptake of 2-[^{3}H]deoxyglucose (2-DOG) using L-[^{14}C]glucose as a measure of the amount of extracellular 2-DOG not removed by washing. In standard experiments, cells were washed three times with buffer A [NaCl (131.5 mM), KCl (4.7 mM), $CaCl_2$ (2.5 mM), $MgSO_4$ (1.25 mM), NaH_2PO_4 (2.5 mM), glucose (5.5 mM), BSA (1 mg/mL), and Hepes buffer (20 mM, pH 7.4)] and then incubated for 20 min in buffer A supplemented with inhibitor (added in DMSO at 1000 times the desired final concentration). After 20 min, insulin was added, and 30 min later, the extent of 2-DOG uptake was measured over 3 min. Effects of insulin were measured at hormone concentrations determined to produce an approximate 50% maximal effect on 2-DOG uptake (0.3 nM for 3T3-L1 adipocytes and 10 nM for L6 myocytes). Data were normalized for recovered cell protein.

Oocytes were removed surgically as clusters from tricaine-anesthetized adult female *Xenopus laevis* (Nasco, Fort Atkinson, WI) that had been primed 3 days earlier with 50 units of pregnant mare's serum gonadotropin injected into the dorsal lymph sac. Oocyte clusters were placed into ice-cold ND96 medium [Hepes (5 mM, pH 7.4), NaCl (96 mM), KCl (2 mM), $MgCl_2$ (1 mM), $CaCl_2$ (1.8 mM), and sodium pyruvate (2.5 mM)]. Oocyte clusters were then rinsed three times in Ca-free ND96, and stage V/VI oocytes were isolated by a combination of mild collagenase treatment (Sigma C-9891 collagenase, 2 mg/mL in Ca-free ND96) and

[2] The 2-carboxymethoxybenzoic acid bioisostere for phosphotyrosine was reported independently by Burke et al. (*18*).

mechanical teasing with watchmaker's forceps. The oocytes were microinjected (in Ca-free ND96) as described previously (*26*) using 92 nL of recombinant PTP1B (150 ng), antibody against PTP1B (clone FG6-1G, Oncogene Research Products) (42 ng), and the PTP1B inhibitor (at various concentrations) in various combinations. Oocytes (18−24 for each experimental condition) were incubated in modified ND96 buffer (K-free to promote insulin-induced oocyte maturation) supplemented with insulin at various concentrations in 60 mm plastic culture dishes at 17 °C and high relative humidity. After 18, 24, and 48 h, oocytes were scored for germinal vesicle breakdown (GVBD) by two investigators. Because of seasonal and individual variability among frogs, the rate and extent of GVBD varied substantially between experiments so that comparing data sets from different experiments was not practical. Therefore, the data are presented as average % GVBD from individual experiments that were qualitatively similar.

Assessment of PTP1B−IR Binding. Insulin receptors were solubilized from CHO cells expressing human insulin receptors (CHO.hIR cells kindly provided by J. Pessin, The University of Iowa, Iowa City, IA) and captured on scintillation proximity assay (SPA) beads coated with wheat germ lectin as described elsewhere (*3*). Binding of [^{35}S]PTP1B^{C215S} (prepared as described above) to the IR on SPA beads was assessed in the absence and presence of PTP1B inhibitors as described previously (*3*).

Measurement of IR Tyrosine Kinase (IRTK) Activity. 3T3-L1 adipocytes were washed three times in buffer A (see above) and then incubated for 31 min in buffer A at 37 °C. During the final 1 min of this incubation, insulin was present at various concentrations. Following insulin stimulation, the cells were washed with ice-cold Dulbecco's phosphate-buffered saline, then lysed in lysis buffer [Hepes (50 mM, pH 7.6), NaCl (150 mM), Triton X-100 (1%), EDTA (5 mM), $Na_4P_2O_7$·$10H_2O$ (20 mM), NaF (100 mM), Na_3VO_4 (1 mM), benzamidine (5 mM), PMSF (1 mM), pepstatin A (1 μM), leupeptin (10 μM), and aprotinin (0.05 TIU/mL)], and centrifuged at 12000*g*. The resulting supernatant fraction (approximately 0.3 mg of protein) was added to 25 μL of wheat germ lectin Sepharose 6MB beads (Amersham Pharmacia Biotech) and mixed for 2−4 h at 4 °C. Beads were then washed twice with lysis buffer and twice with Hepes (60 mM, pH 7.5). Tyrosine kinase activity of the captured IR was measured directly on the beads. Tyrosine kinase assay mixtures contained, in a total volume of 30 μL, Hepes (20 mM, pH 7.5), $MgCl_2$·$6H_2O$ (10 mM), $MnCl_2$·$4H_2O$ (2 mM), [γ-^{33}P]ATP (0.05 mM, 4 Ci/mmol), and the biotinylated peptide substrate (biotin-MAAEEEYMMMMAKKK-NH_2) (24 μM). This peptide sequence is derived from a preferred substrate for IRTK (*27*). Kinase reactions were conducted for 15 min at room temperature and then terminated with the addition of 15 μL of guanidine-HCl (7.5 M). Aliquots of the quenched reaction mix were transferred to 96-well biotin capture plates (Promega). Microtiter plates were washed; scintillation fluid was added, and the amount of ^{33}P was measured in a TopCount scintillation spectrometer (Packard Instruments).

Western Blot Analysis. L6 myocytes and 3T3-L1 adipocytes, which had been exposed to insulin and PTP1B inhibitors at various concentrations, were washed with ice-cold Dulbecco's phosphate-buffered saline and then lysed in 0.35 mL of RIPA buffer [Tris-HCl (50 mM, pH 7.4), NaCl (150 mM), NaF (100 mM), $Na_4P_2O_7$·$10H_2O$ (20 mM), Na_3VO_4 (1 mM), EGTA (1 mM), $(NH_4)_2MoO_4$ (1 mM), NP40 (1%), sodium deoxycholate (0.25%), benzamidine (5 mM), PMSF (1 mM), pepstatin A (1 μM), leupeptin (1 μM), and aprotinin (1 μM)]. Lysates were centifuged (10000*g* for 10 min), and aliquots of each resultant supernatant were mixed in equivalent amounts of protein with Laemmli sample buffer. Proteins were resolved using SDS−PAGE on 8 to 16% gels, electrotransferred to PVDF membranes, and Western blotted for phosphotyrosine using monoclonal antibody 4G10 (Upstate Biotechnology Inc.).

Cocrystallization of PTP1B−Inhibitor Complexes. Cocrystals of PTP1B (amino acids 1−298) with individual inhibitors were grown by hanging drop vapor diffusion at 4 °C using conditions modified from those of Jia et al. (*28*). A stock solution of 15 mg/mL PTP1B (pMB562) in Tris (25 mM, pH 7.5), NaCl (0.3 M), DTT (3 mM), and EDTA (5 mM) was prepared, to which 5 mM inhibitor was added. For crystal growth, a 3 μL drop of stock solution was mixed with an equal volume of precipitating solution [polyethylene glycol 8000 (Fluka) (14−20%), magnesium acetate (0.2 M), cacodylate (0.1 M, pH 6.5)] and equilibrated against 1 mL of the precipitating solution. The orthorhombic crystals (space group $P2_12_12_1$) of PTP1B−inhibitor complexes appeared within 7−14 days.

X-ray Diffraction Data Collection and Processing. Single crystals (approximately 0.3 mm × 0.3 mm × 0.2 mm) were momentarily transferred to a cryoprotectant solution [glycerol (50%), polyethylene glycol 8000 (14%), magnesium acetate (0.1 M), and Hepes (0.1 M, pH 7.5)]. The crystals were then transferred to a loop and flash-frozen in a stream of nitrogen gas at ∼100 K. Data for the PTP1B−compound **VIII** complex were collected at the IMCA beamline at the Advanced Synchrotron Source, Argonne, IL. Data for the PTP1B−compound **VI** complex were collected on a Rigaku RU-300 generator and Raxis IV area detector and processed using the HKL software package (*29*).

Structure Solution. Because the PTP1B−compound **VIII** cocrystals obtained were of a space group different from the space group of those reported by Jia et al. (*28*), the position of the single PTP1B molecule within the orthorhombic cell was determined by molecular replacement using the program AmoRe (*30*). The published PTP1B crystal structure (1ptv) was used as the search model, and data between 15 and 3.0 Å resolution gave an unambiguous solution with a correlation coefficient of 61% and an R_{factor} of 40.8%. Several subsequent cycles of rigid body refinement with X-PLOR (*31*) reduced the R_{factor} slightly to 39.1% for data from 50.0 to 3.0 Å. Examination of $2F_o - F_c$ and $F_o - F_c$ electron density maps at this stage showed clear density for the inhibitor in the active site of the enzyme. It was clear from the initial inspection that the mobile active site loop was not in the expected "down" or closed position, but rather in the "up" or open conformation previously observed for the unliganded PTP1B. Subsequent refinement with REFMAC (*32*) alternated with rounds of manual rebuilding within the program O (*33*) resulted in a model comprising residues 2−298, 462 ordered water molecules identified by the program wARP (*34*), and one inhibitor molecule. Using all data from 50 to

Table 1: K_i Values for Inhibition of Rat PTP1 and Human PTP1B by CCK-8 Analogues

compound	K_i (μM), rat PTP1
H-Asp-Tyr(SO_3H)-Met-Gly-Trp-Met-Asp-Phe-NH_2 (CCK-8)	34
H-Asp-Tyr-Met-Gly-Trp-Met-Asp-Phe-NH_2 (desulfo-CCK-8)	inactive
CCK-8 analogues	
N-acetyl-Asp-Tyr(SO_3H)-Nle-Arg-Trp-Nle-Asp-Phe-NH_2	7
N-acetyl-Asp-Tyr(SO_3H)-Nle-D-Arg-Trp-Nle-Asp-Phe-NH_2	13
N-acetyl-Asp-Tyr(SO_3H)-Nle-D-His-Trp-Nle-Asp-Phe-NH_2	6
N-acetyl-Asp-Tyr(SO_3H)-Nle-Gly-Trp-Nle-Asp-Phe-NH_2	14
N-acetyl-Asp-Tyr(SO_3H)-Nle-Gly-Trp(CHO)-Nle-Asp-Phe-NH_2	6
N-acetyl-Tyr(SO_3H)-Nle-Gly-His-Nle-Arg-NH_2	>100
N-acetyl-Asp-Tyr(SO_3H)-Nle-Gly-Trp-Nle-Arg-Phe-NH_2	11
N-acetyl-Asp-Tyr(SO_3H)-Nle-Gly-His-Nle-Asp-Phe-NH_2	4
consensus tripeptide	
N-acetyl-Asp-Tyr(SO_3H)-Nle-NH_2 (compound **I**)	5
P(+1) analogue of compound I	**K_i (μM), human PTP1B**
N-acetyl-Asp-Tyr(SO_3H)-Nle-NH_2 (compound **I**)	17
N-acetyl-Asp-Tyr(SO_3H)-Ile-NH_2	117
N-acetyl-Asp-Tyr(SO_3H)-Leu-NH_2	95
N-acetyl-Asp-Tyr(SO_3H)-Lys-NH_2	154
N-acetyl-Asp-Tyr(SO_3H)-Glu-NH_2	33

1.8 Å together with an isotropic bulk solvent model yielded a final crystallographic R_{factor} of 18.7% (R_{free} = 24.9%) with good geometry.

As the PTP1B−compound **VI** cocrystals were obtained in the same crystal form as those for the compound **VIII** complex, the latter minus the inhibitor and mobile loop was used as the initial model. After several cycles of rigid body refinement with X-PLOR (*31*), the initial R_{factor} was reduced slightly to 39.0%. Examination of $2F_o - F_c$ and $F_o - F_c$ electron density maps at this stage showed clear density for the inhibitor in the active site of the enzyme and also indicated that the loop was in the down or closed position. Subsequent refinement with REFMAC (*32*) alternated with rounds of manual rebuilding within the program O (*33*) resulted in a model comprising residues 2−298, 108 ordered water molecules identified by the program wARP (*34*), and one inhibitor molecule. Using all data from 50 to 2.2 Å together with an isotropic bulk solvent model yielded a final crystallographic R_{factor} of 19.3% (R_{free} = 26.1%) with good geometry.

Chemistry. The sulfotripeptides (other than compound **I**) were custom synthesized by AnaSpec Inc. (San Jose, CA). Preparation of other compounds is described elsewhere (*21*, *35*).

RESULTS

CCK-8 Analogues Inhibit PTP1B. Cys^{215} of PTP1B, which is essential for catalysis, likely exists as a thiolate anion at physiologic pH and is highly reactive (*36*, *37*). It was anticipated, therefore, that in a search for small molecule inhibitors of PTP1B a large number of undesirable covalent modifiers of Cys^{215} would be uncovered. For that reason, PTP1B assays were conducted in the presence of DTT (1 mM). Nevertheless, many of the inhibitors identified were found to irreversibly inhibit PTP1B by reacting with Cys^{215}, and these included several classes of compounds, e.g., 1,4-benzoquinones that are known inhibitors of cysteine proteases (*38*). Therefore, we used an alternate strategy of targeted screening of compounds that contained known or suspected phosphotyrosine bioisosteres and identified a series of sulfotyrosyl-containing octapeptides that were potent inhibitors of PTP1B (Table 1). These octapeptides were analogues of CCK-8, and it was found that CCK-8 itself, but not desulfo-CCK-8, also inhibited PTP1B. Not all of the CCK-8 analogues that were tested inhibited PTP1B, and of those which were inhibitory, all contained the N-terminal tripeptide sequence *N*-acetyl-Asp-Tyr(SO_3H)-Nle-. Synthesis of the C-terminal amide of this common tripeptide, compound **I**, confirmed that this sulfotripeptide was sufficient for inhibitory activity, and it competitively inhibited recombinant rat PTP1B with a K_i value of 5 μM. This potency was unexpected on the basis of previous reports that at least six amino acids were required for a high-affinity substrate (*39*), but is consistent with a subsequent report that smaller sulfopeptides can be effective inhibitors of PTP1B (*40*). Compound **I** was slightly less potent at inhibiting recombinant human PTP1B (K_i = 17 μM). Substitution of Ile, Leu, or Lys for Nle in the P(+1) position resulted in significant loss of potency, while substitution with Glu was better tolerated (Table 1). One of the proposed targets of PTP1B, pY^{1158} of the β-subunit of the insulin receptor, is flanked by Glu^{1159} in the P(+1) site (*41*).

Evolution of Analogues of Compound I. Because neither a sulfotyrosyl group nor a peptide bond is pharmacokinetically desirable in a potential drug, we chemically modified compound **I** to introduce a stable phosphotyrosine bioisostere and to minimize peptidic characteristics. Some of the modifications utilized in the evolution of compound **I** are summarized in Figure 1. Removal of the two terminal amide moieties afforded the bis(amide) compound **II** which retained remarkable potency (K_i = 30 μM), encouraging us to attempt further modifications. Replacement of the *O*-sulfate with the known phosphate bioisostere *O*-malonate (*42*) then provided compound **III**, which proved to be significantly more potent than the corresponding sulfate. The activity of compound **III** could be augmented by the insertion of a phenylalanine unit into the N-terminus (compound **IV**, K_i = 1.2 μM), or by introduction of a novel phosphotyrosine bioisostere, 2-carboxymethoxybenzoic acid (compound **V**, K_i = 2.8 μM) (*21*). Combining these two useful modifications yielded a compound (**VI**) that inhibited competitively with submicromolar potency (K_i = 0.25 μM) (Figure 1). Alternatively, the

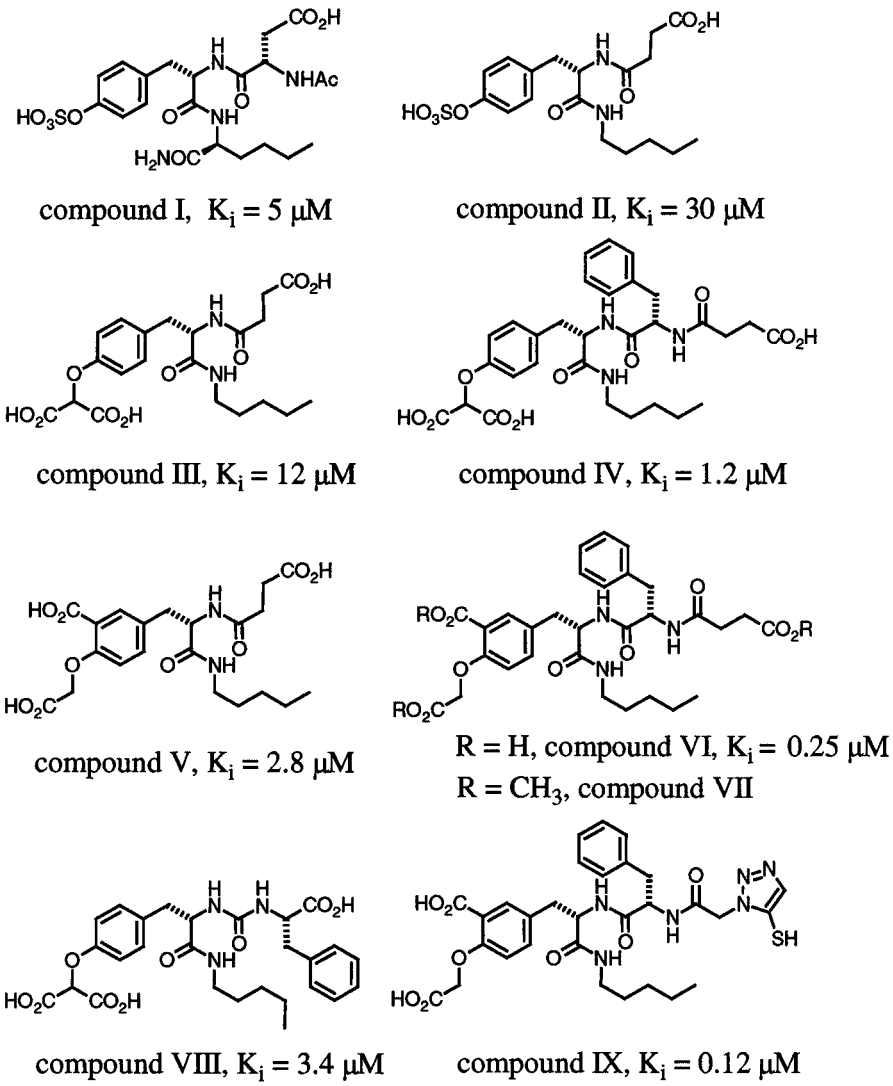

FIGURE 1: Key compounds in the evolution of potent PTP1B inhibitors derived from the CCK-8-related sulfotyrosyl tripeptide, compound **I**. Each of the compounds that is shown was found to be a competitive inhibitor of PTP1B with the indicated K_i value. Each compound was also tested at 1, 10, and 100 μM for inhibition of LAR, SHP-2, cdc25b, and calcineurin and was either inactive or inhibited <20% at 100 μM. Each compound inhibited PTP1B and TC-PTP with approximately equal potency.

peptidic nature of compound **III** could be decreased by replacing one of the amides with a urea while incorporating the phenylalanine unit, affording compound **VIII** (K_i = 3.4 μM). Substitution of the N-terminal carboxyl group with a surrogate 5-sulfanyl-1*H*-1,2,3-triazole yielded compound **IX**, a competitive inhibitor with a K_i value of 0.12 μM. None of the compounds in Figure 1 displayed significant selectivity for PTP1B over TC-PTP, the known PTP that is structurally the most similar to PTP1B, but they all inhibited <20% at 100 μM when tested against LAR and SHP-2, two PTP enzymes more distantly related to PTP1B. Likewise, these compounds were poor inhibitors of either calcineurin or cdc25b. All these compounds also inhibited PTP1B-catalyzed hydrolysis of TRDI(pY)ETD(pY)(pY)RK, a phosphopeptide that matches a sequence within the activated kinase domain of the insulin receptor β-subunit. The kinase domain phosphopeptide was not used routinely to define kinetics of inhibition because, first, the malachite green assay employed to measure the rate of inorganic phosphate release was not sensitive enough to allow measurements of accurate K_m values for the phosphopeptide and, second, the nonequivalence of the three phosphotyrosines in the peptide with respect to PTP1B-catalyzed hydrolysis (*5*) complicated the interpretation of inhibitor kinetics.

In Vitro Activities of PTP1B Inhibitors. Compound **VI**, a potent triacid inhibitor of PTP1B, completely inhibited PTP1B by binding in the catalytic pocket in a manner defined using X-ray crystallography (see below). Binding of compound **VI** in the catalytic pocket of PTP1B blocked the interaction of PTP1B with intact insulin receptors captured on lectin-coated SPA beads. For this assay, PTP1B was ^{35}S-labeled and rendered catalytically inactive by mutating Cys^{215} to Ser^{215}. Compound **VI** competitively displaced [^{35}S]-$PTP1B^{C215S}$ from immobilized insulin receptors with a K_i value (0.28 μM) that was almost identical to that observed for inhibition of PTP1B-catalyzed hydrolysis of pNPP (0.25 μM) (Figure 2). These data complement other data that indicate the catalytic site of PTP1B is the principal domain of the enzyme involved in binding to insulin receptors, at least under these in vitro conditions, and that blocking the active site effectively disrupts PTP1B−IR binding (*3*).

Binding of catalytically competent PTP1B to the activated (tyrosine-phosphorylated) IR results in receptor dephosphorylation (*3*, *5*). To determine whether the small molecule

Table 2: Evidence That Compound **VII** Enters Cells and Is a Substrate for Esterase(s) Which Generate Products That Inhibit PTP1B Activity[a]

	compound **VI**	compound **VII**
K_i (μM) for PTP1B inhibition	0.25	no inhibition at 100 μM
Caco-2 cell permeability coefficient (absorptive, nm/s)	<0.3	136 ± 7.3

Esterase-Treated Compound **VII**		
treatment time (h)	% inhibition of PTP1B	inhibitor composition
0	0	TME (100%)
1	23 ± 0.8	TME (1%), DME[b] (76.4%), MME[c] (22.6%), free acid (trace)
12	43 ± 5	TME (2.9%), DME (40.2%), MME (56.9%), free acid (trace)

[a] For the esterase treatment, the trimethyl ester (TME) compound **VII** (1 mM) was incubated at room temperature with porcine hepatic esterase coupled to acrylic beads in 50 mM Tris-HCl buffer (pH 8.2) for either 1 or 12 h. Portions of the reaction mixture were tested for their ability to inhibit PTP1B-catalyzed hydrolysis of pNPP, and other portions were subjected to HPLC and LC−MS/MS analysis. [b] Dimethyl ester (DME) isomers yielding the expected peak at MH^+ 628. MS/MS showed clearly that the N-terminal methyl group was retained but did not allow assignment of the second methyl group to one of two possible positions within the phosphotyrosine bioisostere. [c] Monomethyl (MME) isomers yielding the expected MH^+ 614. Two of the three possible monomethyl esters were resolved. Changes in MS/MS peak intensities at *m*/*z* 367, 335, 248, and 252 ruled out the retention of the N-terminal methyl group but did not allow assignment of the methyl group to one of the two possible positions within the phosphotyrosine bioisostere.

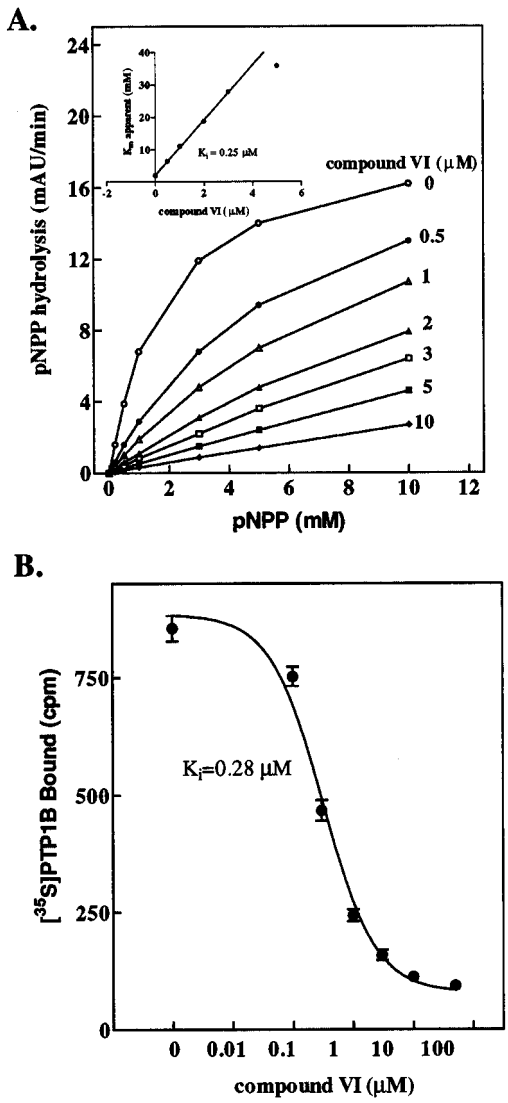

FIGURE 2: Inhibition of PTP1B-catalyzed hydrolysis of pNPP and PTP1B binding to the IR by compound **VI**. The K_i value for inhibition by compound **VI** of PTP1B-catalyzed hydrolysis of pNPP was determined using the direct linear method of Cornish-Bowden (Materials and Methods). Data for competitive displacement of [^{35}S]PTP1B^{C215S} from the IR immobilized on WGA-SPA beads were fitted to a model of single-site competition to yield the K_i value that is shown. Data are from two typical experiments.

inhibitors of PTP1B identified here could protect against the loss of IR tyrosine kinase (IRTK) activity that accompanies PTP1B-dependent dephosphorylation of the receptors, IRs were first partially purified from 3T3-L1 adipocytes that had been exposed to insulin at various concentrations. Tyrosine kinase activity of the partially purified IR was measured using as a substrate a biotin conjugate of a peptide based on an optimal substrate for the IRTK (*27*). IRTK activity was increased dose-dependently up to 10-fold when cells were exposed to insulin (Figure 3A,B). Treatment of insulin-activated IR with recombinant PTP1B reduced IRTK activity to a basal (nonstimulated) level (Figure 3C). However, pretreatment of the PTP1B with various inhibitors resulted in partial conservation of IRTK activity (Figure 3D). The extent to which various inhibitors protected against PTP1B-catalyzed loss of IRTK activity correlated with their potencies (K_i values) for inhibiting PTP1B-catalyzed hydrolysis of pNPP (Figures 1 and 3D).

Cell Activities of PTP1B Inhibitors. The PTP1B inhibitors shown in Figure 1 are sufficiently polar that they would be expected to penetrate cells poorly by passive diffusion, and this was confirmed using Caco-2 cells (unpublished data and Table 2). Therefore, preliminary determination of the effects of these PTP1B inhibitors on insulin signaling in cells was accomplished by microinjecting the inhibitors into *Xenopus* oocytes. Insulin has been shown to promote oocyte maturation [monitored as increased germinal vesicle breakdown (GVBD)], and this process is antagonized by PTP1B (*43*). We were able to immunoprecipitate a protein from oocyte lysates using a monoclonal antibody (clone FG6-1G, Oncogene Research Products) against human PTP1B which, on Western blots, migrated with an estimated size of 43 kDa. When the PTP1B antibody (42 ng) was microinjected into oocytes, there was an augmented insulin-induced GVBD, while conversely, microinjection of recombinant PTP1B (150 ng) attenuated this insulin response (Figure 4A). Microinjection of a PTP1B inhibitor, compound **IX** (100 pmol), mimicked microinjection of the PTP1B antibody and potentiated insulin-induced GVBD. Co-injection of compound **IX** with PTP1B partially protected against the loss of insulin-induced GVBD caused by PTP1B (Figure 4B).

All the PTP1B inhibitors in Figure 1 were tested for effects on insulin-stimulated glucose transport (2-DOG uptake) by 3T3-L1 adipocytes and L6 myocytes. Most had little or no

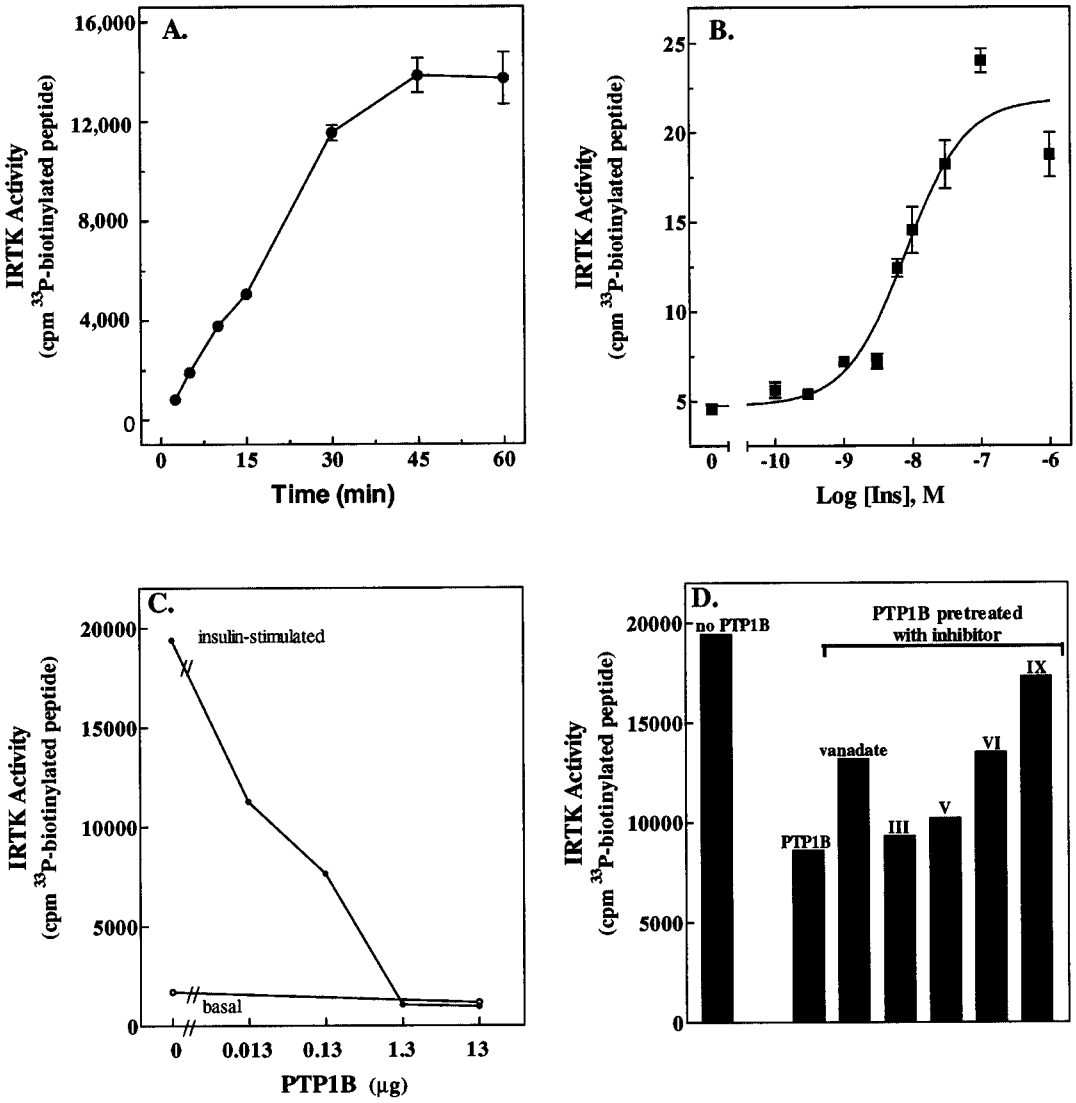

FIGURE 3: Effects of insulin, PTP1B, and inhibitors of PTP1B on IRTK activity. 3T3-L1 adipocytes were treated with insulin for 1 min, and then the cells were lysed and insulin receptors partially purified using beads coated with wheat germ lectin. IRTK activity of the bead-immobilized insulin receptors was assayed at ambient temperature for 15 min using a biotinylated peptide as the substrate (Materials and Methods). (A) Kinetics of phosphorylation of biotinylated peptide by insulin receptors isolated from insulin-treated cells. (B) Insulin-dependent increases in IRTK activity of insulin receptors isolated from 3T3-L1 adipocytes exposed to insulin at various concentrations. (C) PTP1B-dependent loss of IRTK activity of insulin receptors isolated from insulin-treated cells. Activated insulin receptors were pretreated for 10 min with PTP1B. Pretreatment was terminated by addition of vanadate, and IRTK assays were performed. (D) Preservation of IRTK activity by selected PTP1B inhibitors. PTP1B-catalyzed dephosphorylation of activated insulin receptors was inhibited by inclusion of inhibitors, present at 100 μM, during the pretreatment phase. Data are mean values ± standard error of the mean ($n = 3$) derived from typical experiments.

effect, most likely because they failed to significantly enter the cells. Compound **VI**, even at 100 μM, had no effect on insulin-dependent 2-DOG uptake by L6 myocytes (Figure 5A). In contrast, the trimethyl ester of this inhibitor, compound **VII**, increased the rate of 2-DOG uptake in either the absence or presence of insulin at a submaximal concentration (10 nM) (Figure 5B). In the presence of compound **VII**, the stimulation of 2-DOG uptake by insulin (10 nM) was now similar to that observed with a maximally effective concentration of insulin (300 nM). These effects of compound **VII** on 2-DOG uptake were accompanied by an increased level of tyrosine phosphorylation of the IR, and IRS-1 and IRS-2 (Figure 5B). Importantly, compound **VII** also exhibited activity in a cell model of insulin resistance. 3T3-L1 adipocytes that are exposed overnight to high levels of glucose (25 mM) and insulin (100 nM) (HGI-treated) exhibit attenuated responses to insulin. Compound **VII** augmented insulin-dependent 2-DOG uptake by HGI-treated 3T3-L1 adipocytes (Figure 5C). At 0.1 nM insulin, compound **VII** approximately doubled the rate of 2-DOG uptake, but with 3 nM insulin, it no longer had an effect. These data are consistent with the hypothesis that inhibition of PTP1B enhances potency but not efficacy of insulin in this cell model. These compound **VII**-induced changes in 2-DOG uptake were accompanied by an increased level of tyrosine phosphorylation of the IR and IRS-1 (Figure 5D).

Compound **VII** at concentrations up to 100 μM, however, did not inhibit the hydrolysis of pNPP catalyzed by recombinant PTP1B (Table 2). This suggested that compound **VII** entered L6 myocytes and 3T3-L1 adipocytes and was then

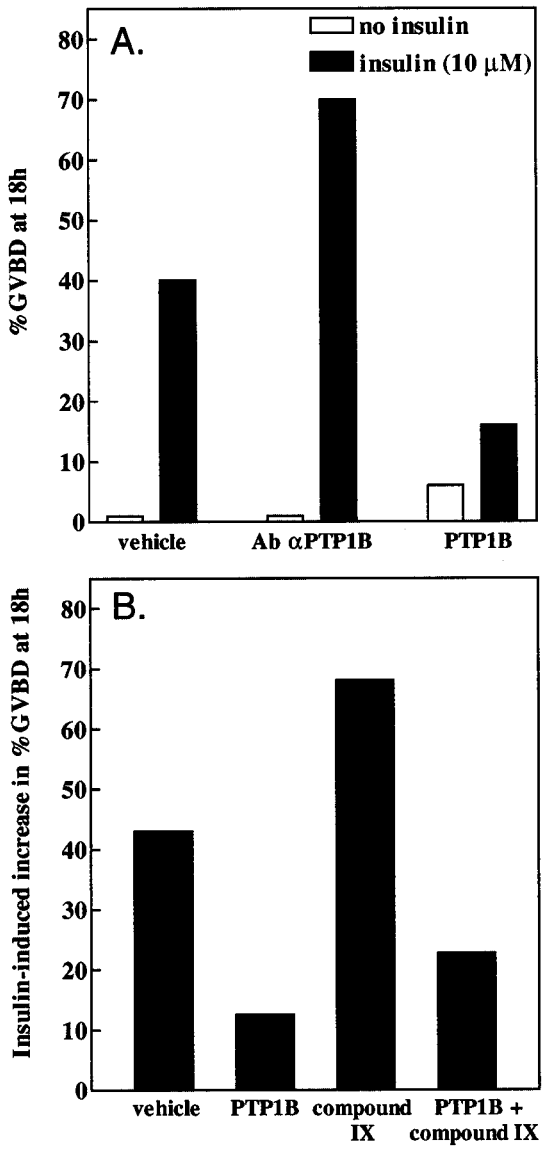

FIGURE 4: Effect of a PTP1B inhibitor on insulin-dependent germinal vesicle breakdown in *Xenopus* oocytes. Stage V/VI oocytes from gonadotropin-primed frogs were injected (92 nL) with either PTP1B (150 ng), antibody F6G-1G against PTP1B (42 ng), or compound **IX** (100 pmol, alone and with PTP1B). Each experimental group contained 18−24 oocytes. Injected oocytes were returned to medium supplemented with insulin (5 μM), and after 18 h, two investigators independently scored the cells for germinal vesicle breakdown (GVBD). Data are percentages of cells exhibiting GVBD and are from a typical experiment.

hydrolyzed to generate a PTP1B inhibitor. Measurements of Caco-2 cell penetration by compounds **VI** and **VII** were consistent with the likelihood that the more lipophilic compound **VII** readily enters cells (Table 2). Once inside the cell, it seems unlikely that compound **VII** would be completely de-esterified to compound **VI** based on known esterase specificities (*44*). Indeed, using porcine hepatic esterase as a model esterase, even prolonged incubation of compound **VII** with esterase failed to generate detectable compound **VI** (Table 2). However, mass spectrometric analysis revealed generation of both mono- and dicarboxylic acid derivatives from compound **VII** that had been treated with esterase. Furthermore, esterase treatment of compound **VII** yielded a mixture of products that now inhibited PTP1B-catalyzed hydrolysis of pNPP (Table 2).

Table 3: PTP1B−Inhibitor Crystallographic Data and Refinement Statistics[a]

	compound **VIII**	compound **VI**
crystal data		
space group	$P2_12_12_1$	$P2_12_12_1$
unit cell (Å)	$a = 52.7$, $b = 83.8$, $c = 88.7$	$a = 52.9$, $b = 82.4$, $c = 88.6$
resolution (Å)	1.8	2.2
no. of total measurements	643419	249675
no. of unique reflections	37591	17760
% complete	97.3 (50−1.8 Å)	87.6 (50−2.2 Å)
% complete	97.0 (2.0−1.8 Å)	65.1 (2.5−2.2 Å)
R_{sym}[b]	0.067	0.089
refinement parameters		
no. of protein and ligand atoms	2928	2580
Δ bond (Å)	0.011	0.019
Δ angle (deg)	1.2	1.4
resolution (Å)	50.0−1.8	50.0−2.2
no. of reflections	33641	17733
R_{cryst}[c]	0.187	0.202
R_{free}	0.249	0.261

[a] All recorded reflections were used during maximum likelihood refinement in REFMAC. The quoted R_{factor} values were calculated using all data. [b] $R_{sym} = \sum\sum(|I_{hi}| - |I_h|)/\sum_{hi} I_{hi}$, where I_{hi} and I_h are the intensities of the individual and mean structure factors, respectively. [c] $R_{cryst} = \sum|F_o| - |F_c|/\sum F_o$. Only data with $F_o/\sigma(F_o) > 2.0$ were used in the refinement.

Structure Solution of PTP1B−Inhibitor Complexes. Table 3 summarizes crystallographic data and refinement statistics for two PTP1B−inhibitor complexes that represent the two binding modes that were discovered within this series of structurally related PTP1B inhibitors. In one mode, typified by compound **VIII**, the WPD loop (encompassing residues 179−189) is in the open conformation in the PTP1B−inhibitor complex, while in the other mode typified by compound **VI**, the WPD loop is closed. However, despite the differences in the conformation of the WPD loop, the overall modes of binding of compounds **VIII** and **VI** to PTP1B are quite similar (Figures 6 and 7). For both compounds, the peptide backbone portion of the inhibitors forms an extended β-strand conformation closely resembling that seen previously for PTP1B−phosphotyrosine (pTyr) peptide structures (28). Both compounds maintain two conserved hydrogen bonds between the Asp[48] side chain and the main chain nitrogens on either side of the central pTyr side chain mimic [P and P(+1) positions] and a third between the main chain nitrogen of Arg[47] and a main chain carbonyl of the inhibitor at the P(−2) position. The phenyl rings of the two pTyr side chain mimics also make similar hydrophobic packing interactions with the side chains of Tyr[46], Val[49], Ala[217], Ile[219], and Gln[262], though in the case of compound **VI** the closure of the WPD loop results in an additional interaction with Phe[182]. In addition, the C-terminal pentyl chain [P(+1)] of both compounds lies in a shallow hydrophobic pocket and forms hydrophobic contacts with the side chains of Val[49], Ile[219], and Gln[262] (Figure 7).

As reported recently (*54*), compared to the PTP1B−peptide structures which contain an acidic residue at the P(−1) position, the Phe residue at this location in compounds **VI** and **VIII** induces a repositioning of the Arg[47] side chain (5 and 7 Å shift in the guanidinium carbon, respectively), thus permitting hydrophobic interactions with the aliphatic portions of Arg[47] and Asp[48]. Furthermore, despite the

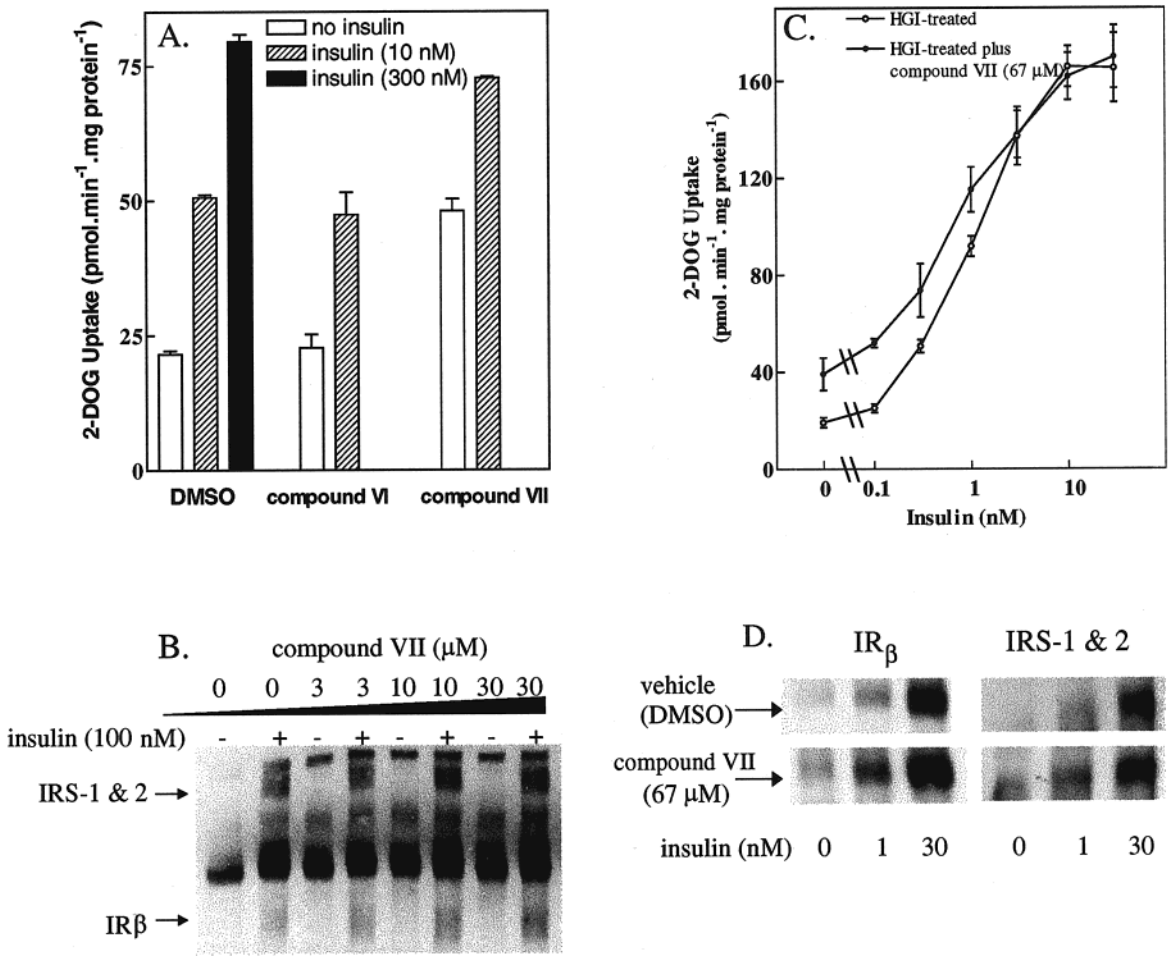

FIGURE 5: Effects of compound **VI** and its triester, compound **VII**, on insulin-dependent 2-DOG uptake and tyrosine phosphorylation of insulin signaling molecules in L6 myocytes and insulin resistant 3T3-L1 adipocytes. L6 myocytes that had been washed and maintained for 5 h in serum-free medium [αMEM with BSA (1 mg/mL)] were treated with either compound **VI** (100 μM), compound **VII** (100 μM), or vehicle (0.1% DMSO) (A) or compound **VII** at various concentrations (B) for 20 min before the addition of insulin at concentrations that elicited an approximate half-maximal insulin response (10 nM) or a full response (300 nM). After an additional 30 min, either 2-DOG uptake was assessed (A) or cells were lysed and phosphotyrosine Western blots of lysate proteins were performed (B). 3T3-L1 adipocytes were rendered insulin resistant by incubation overnight in medium supplemented with high glucose (25 mM) and insulin (100 nM). Insulin-dependent 2-DOG uptake (C) and tyrosine phosphorylation (D) were then assessed (Materials and Methods). In some dishes of cells, compound **VII** (67 μM) was present throughout the experiment.

structural differences at the P(−2) positions of the two inhibitors, the flexibility of the Arg[47] side chain allows the guanidinium group to interact favorably with the negatively charged terminal carboxylates as well as to accommodate the hydrophobic residue at the P(−1) position (Figures 6 and 7).

In the known PTP1B−pTyr peptide crystal structures, two of the phosphate oxygen atoms of the pTyr residue make two hydrogen bonds each to the main chain amides of Ser[216] and Ala[217], and Ile[219] and Gly[220] (*28*). The phosphate mimic headgroups of both compounds **VI** and **VIII**, however, are positioned somewhat closer to the WPD loop than the phosphate group of the bound substrate, resulting in the loss of two (compound **VIII**) or all four (compound **VI**) of these hydrogen bonds. These lost interactions with the backbone amides are instead made to new structurally bound water molecules. The positioning of the headgroups closer to the WPD loop in both complexes also results in the displacement of a bound water molecule hydrogen bonded to Glu[266] in the PTP1B−substrate structures with compensatory hydrogen bonds being formed by headgroup oxygens (Figures 6 and 7).

The differences in the binding modes of these two compounds with regard to the conformation of the WPD loop are also a direct consequence of the differences in the nature of the headgroups of the these two compounds.

*Binding Mode of Compound **VIII***. In general, the binding of the *O*-malonyltyrosyl (OMT) side chain resembles that previously observed by Groves et al. (*46*) for the *O*-fluoromalonyltyrosine cyclic peptide (FOMT). In particular, the Arg[221] side chain and WPD loop adopt the open conformation characteristic of the unliganded state of PTP1B (Figure 6). However, the phenyl ring of the *O*-malonyltyrosyl side chain in compound **VIII** penetrates about 1 Å deeper into the binding pocket than FOMT, and in this respect, the binding more closely resembles the binding of a phosphotyrosine residue. When the substrate binds to PTP1B, a concerted conformational change occurs in the positions of Arg[221] and the WPD loop which brings the general acid Asp[181] in the proximity of the ester oxygen of the substrate for efficient catalysis (28). These motions result from the optimization of the hydrophobic packing between the aliphatic portions of the Arg[221] and Trp[179] side chains. The WPD loop is then stabilized in the closed position by (i)

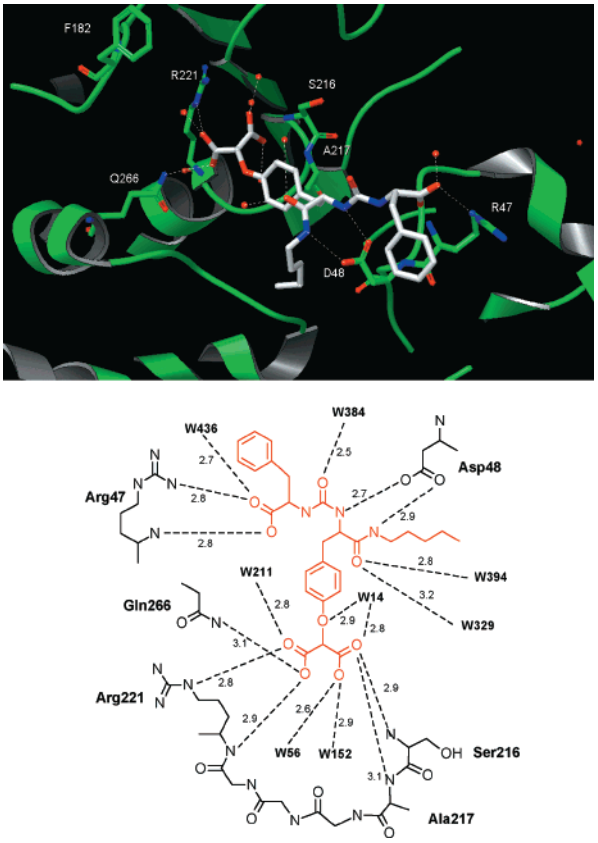

FIGURE 6: PTP1B−compound **VIII** complex. (Top) Ribbon diagram depicting the docking of compound **VIII** (white backbone) into the active site of PTP1B (green). (Bottom) Schematic representation of the interactions between compound **VIII** (red) and key residues in PTP1B (as labeled, W = water). All distances are in angstroms.

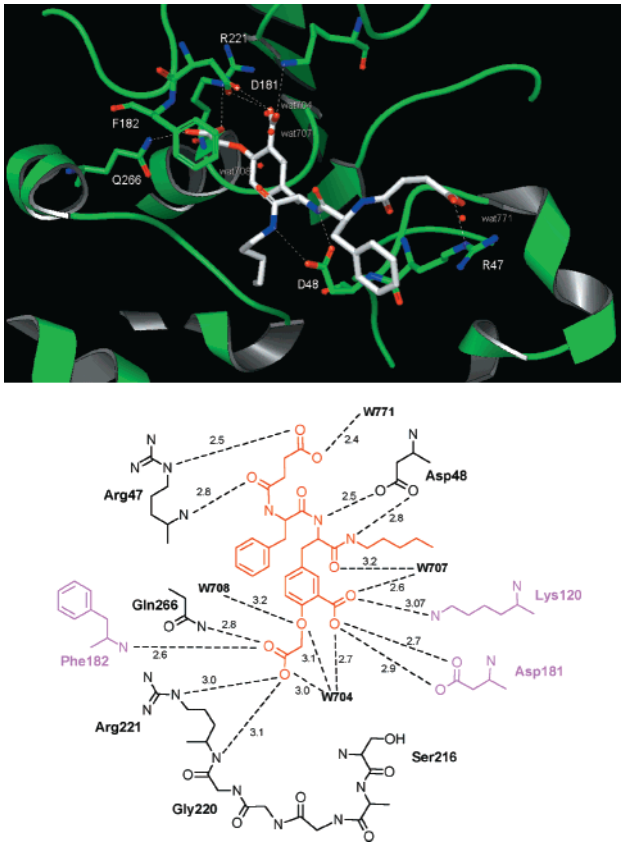

FIGURE 7: PTP1B−compound **VI** complex. (Top) Ribbon diagram depicting the docking of compound **VI** (white backbone) into the active site of PTP1B (green). (Bottom) Schematic representation of the interaction between compound **VI** (red) and key residues in PTP1B (as labeled, W = water). Residues in PTP1B that contribute to binding of compound **VI**, but not to binding of compound **VIII**, are colored magenta. All distances are in angstroms.

hydrogen bonds between the guanidine group of Arg[221] and two phosphate oxygen atoms, (ii) the hydrogen bond between the guanidinyl NH1 of the arginine and the carbonyl oxygen of Pro[180], and (iii) a buried water molecule that links the amide nitrogen of Phe[182], the side chain of Gln[226], and the phenolic oxygen atom of the pTyr group.

In the PTP1B−FOMT crystal structure (*46*), the open conformation was thought to be due to differences in the positions of the oxygen atoms of the malonyl and pTyr phosphate groups causing less favorable hydrogen bonding between the Arg[221] side chain in the WPD loop in the closed conformation. However, because compound **VIII** projects 1 Å deeper into the binding pocket than FOMT, the open conformation would also seem to be at least partly due to steric considerations. In particular, modeling studies show that in the closed conformation there would be close contacts between malonyl oxygen atoms and Arg[221] NH_2 (1.6 Å) and the backbone amide of Phe[182] (2.2 Å).

*Binding Mode of Compound **VI**.* As with the PTP1B−pTyr peptide structures, the binding of compound **VI** is accompanied by closure of the catalytic site WPD loop (Figure 7). However, the side chain of Phe[182] interacts more closely with the phenyl ring of the inhibitor than it does with that of pTyr as a result of a 90° rotation of its Cα−Cβ bond. This conformation of the Phe[182] side chain closely resembles that observed in the PTP1B−(difluoronaphthylmethyl)-phosphonate inhibitor complexes determined by Groves et al. (*46*). In the compound **VI** complex, the position normally taken up by the phosphate group of the pTyr is essentially unoccupied by the inhibitor. Instead, the two phosphate oxygens which hydrogen bond to the main chain amides as described above are both replaced with bound water molecules (W[704] and W[708]) (Figure 7). These solvent molecules form a network of hydrogen bonds between residues of the phosphate binding site (the amides of Ser[216], NH1 of Arg[221] and Ile[219], and Gly[220]) and the ether oxygen of the inhibitor itself. The tyrosine headgroup of compound **VI** is instead located closer to the WPD loop where its terminal carboxylate makes a series of five hydrogen bonds to the main chain nitrogen of Phe[182], the side chain amide of Gln[266], the side chain NE1 and main chain nitrogen of Arg[221], and one of the ordered waters (W[704]) located in the phosphate binding site. The *o*-carboxyl substituent of the inhibitor in turn forms hydrogen bonds to Lys[120] (3.07 Å) and to two water molecules, including W[704]. This *o*-carboxyl is also seen to interact strongly (2.7 Å) with the side chain of Asp[181] presumably by sharing a proton. Such an interaction between two acidic groups is energetically favorable at neutral pH (*46*) and was also observed in the PTP1B−2-(oxalylamino)-benzoic acid crystal structure (*16*).

DISCUSSION

While multiple PTP enzymes may be involved in regulating insulin action (*47*, *48*), there is sufficient evidence that inhibition of PTP1B will augment insulin action to warrant

a search for PTP1B inhibitors. It was generally believed that a small molecule inhibitor that acted by covalently modifying catalytically essential Cys^{215} would be undesirable. However, the experience with cysteine proteases provides precedent for identifying SH reactive inhibitors that retain selectivity (*49*), and it has recently been proposed that controlled oxidation and reduction of Cys^{215} may provide physiological regulation of PTP1B activity (*37*). With the goal of developing reversible, competitive inhibitors of PTP1B, we screened potential pTyr bioisosteres and identified sulfotyrosyl-containing octapeptides that were surprisingly potent PTP1B inhibitors. While these compounds were synthesized originally as CCK-8 analogues, the prototypic nonpeptidic CCKA antagonist, proglumide, had no effect on PTP1B activity (data not shown). Rather, these octapeptides shared a common N-terminus, *N*-acetyl-Asp-Tyr(SO_3H)-Nle-, that was essential and sufficient for inhibition. The tripeptide (compound **I**) inhibited rat PTP1 with a K_i of 5 μM, a potency that was unexpected for a tripeptide in light of previous work suggesting that a hexapeptide was a minimally effective substrate [Ac-DADEpYL-NH_2 was identified as a preferred substrate (K_m = 3.6 μM) (*39*)]. Similarly, compound **I** has an acidic residue at P(−1) and an uncharged residue at P(+1). After our study was completed, Vetter et al. (*51*) reported the use of inverse alanine scanning to confirm the preference of PTP1B for substrates with an acidic P(−1) residue, and they further showed that a methionine in the P(+1) position improves k_{cat}/K_m substantially over all other amino acids, including leucine. This suggests that *N*-acetyl-Asp-Tyr(SO_3H)-Met may have been an even better template from which to design a PTP1B inhibitor. Vetter et al. (*51*) also showed that insertion of a Lys within up to three residues before or after the phosphotyrosine in a peptide greatly diminished its suitability as a substrate for PTP1B. In the study presented here, substitution of Lys for Nle in compound **I** increased K_i approximately 9-fold. There was also a distinct preference for Nle over other uncharged residues. In rank order of increasing K_i values, Nle < Leu < Ile and even Glu at P(+1) yielded an inhibitor more potent than those with either Leu or Ile at P(+1). Desmarais et al. (*40*) also observed a preference for a bulky hydrophobic residue in the P(+1) position of sulfotyrosyl inhibitors, and our results confirm their observation that peptides smaller than six amino acids can have excellent potency [IC_{50} for AcDE(sY)L-Nle = 2 μM]. They examined the elements required for inhibition of PTP1B by sulfotyrosyl peptides based on a known high-affinity phosphotyrosyl peptide from the EGF receptor autophosphorylation site and observed that IC_{50} values for the tetrapeptide AcAsp-Glu-Tyr(SO_3H)-X increased in the following order: X = Nle < Leu < Ile < Val. It has been proposed that the residues immediately C-terminal to the substrate phosphotyrosine make modest van der Waals interactions with hydrophobic residues on the surface of the enzyme (*52*). These interactions may be facilitated by the C-terminal amidation of compound **I** because it was found previously that amidation of the C-terminal free carboxyl of leucine in the EGF receptor-derived substrate DADEpYL increased catalytic efficiency almost 6-fold (*39*). While the van der Waals interactions at P(+1) are energetically small compared to the electrostatic interactions between the negatively charged P(−1) residue and PTP1B, the latter are compensated by solvent interactions with polar residues in the unbound peptide, and it has been argued that the van der Waals interactions make a disproportionate contribution to the overall energy of binding that could be exploited in the design of inhibitors (*52*).

Molecular dynamic simulations have revealed that other sulfotyrosyl peptides bind to PTP1B in an extended β-strand conformation in which only the residues around sulfotyrosine contribute significantly to the binding (*52*). Residues more N-terminal and C-terminal provide stabilizing interactions but are quite fluxional and remain solvent accessible. Most of the PTP1B surface was computed to have a predominantly negative electrostatic field with only the field surrounding the phosphotyrosine binding pocket being positive (*53*). Interaction between Arg^{47} within this positive surface and the negative charge of the P(−1) residue of the substrate has been proposed to be an important determinant of PTP1B substrate specificity (*54*), although it is recognized that a variety of P(−1) residues can be accommodated by PTP1B (*51*).

While structure-based design of inhibitors based on peptide substrates has yielded peptide inhibitors of high potency, peptides have significant disadvantages as therapeutic agents (*13*). An additional limitation of peptide-based inhibitor design was revealed by Gao et al. (*17*), who reported that monocarboxy-based phosphotyrosine mimetics, which can be incorporated into nonpeptidic small molecules to generate potent PTP1B inhibitors, are ineffective when incorporated into peptides. Therefore, beginning with compound **I** as a template, we synthesized analogues with the goals of minimizing peptidic nature, replacing sulfotyrosine with a more stable and pharmacokinetically desirable phosphotyrosine bioisostere, facilitating cell penetration by reducing overall charge, and enhancing lipophilicity, while maintaining a molecular size of <600 Da. These analogues either retained or significantly improved upon the potency of the original tripeptide and did not appreciably inhibit the other phosphatases that were tested. The exception, however, was TC-PTP which was essentially inhibited with equal potency by this series of PTP1B inhibitors. One strategy to gain selectivity for PTP1B over TC-PTP may be to exploit binding at the second low-affinity, noncatalytic, aryl-phosphate binding site on PTP1B described by Zhang and co-workers (*55*), an approach used by those same investigators to design PTP1B selective bis(aryldifluorophosphonates) (*56*). Within the second aryl-phosphate binding site, five residues (R^{254}, M^{258}, G^{259}, Q^{262}, and R^{24}) were identified to be involved in H-bonding interactions with the substrate (*55*). Four of those residues fall in a sequence that is identical in human PTP1B, rat PTP1, mouse PTP1, and human TC-PTP. The fifth residue (R^{24}) is in a sequence that is identical in the human, rat, and mouse forms of PTP1B, but not in TC-PTP. It remains to be determined whether the sequence differences around R^{24} in PTP1B and TC-PTP result in significant structural differences that are accessible and can be exploited by active site-directed inhibitors.

The peptidomimetic PTP1B inhibitors described here inhibit binding of PTP1B to activated insulin receptors with K_i values similar to those determined for inhibition of PTP1B-catalyzed hydrolysis of pNPP, indicating that the catalytic site of PTP1B is likely the principal domain involved in binding. The inhibitors also protect against

PTP1B-induced loss of IRTK activity in a reconstituted system. While the rank order of potency for protection of IRTK activity matched that for inhibition of pNPP hydrolysis, much more inhibitor was required for IRTK protection. This is most likely because these are competitive inhibitors, and therefore, the extent of inhibition is dependent upon the concentration and K_m of the substrate (IR). The K_m of IR for PTP1B is <10% of that of pNPP, and the surface concentration of IRs is likely high following their capture and enrichment on lectin-coated beads.

While the inhibitors described here for the most part have predictably poor cell penetration, they consistently demonstrated augmentation of insulin action when introduced into cells via microinjection, as a lipophilic ester, or by liposomal encapsulation (data not shown for the last case). Glucose uptake was monitored as a pathophysiologically relevant index of insulin action, but it should be noted that this is a downstream response that depends on tyrosine phosphorylation of IR and IRS-1 only over a limited range of phosphorylation levels (*57*). In insulin resistant 3T3-L1 adipocytes, a PTP1B inhibitor augmented insulin-dependent 2-DOG at low insulin concentrations, but this effect was lost when uptake was stimulated maximally with insulin. These findings are consistent with a mechanism by which PTP1B inhibitors increase the potency but not the efficacy of insulin. In the absence of insulin, a PTP1B inhibitor might be expected to be "insulin-mimetic" if the insulin receptor has a basal constitutive tyrosine kinase activity that is normally attenuated by PTP1B. This may account for the observation that, in L6 cells, compound **VII** increased the extent of IR tyrosine phosphorylation and the rate of 2-DOG uptake even in the absence of insulin. In the experiments where insulin action was potentiated by the PTP1B inhibitor, there was an increased level of tyrosine phosphorylation of both IR and IRS-1 and -2. An increased level of IRS-1 phosphorylation could be a consequence of an increased level of IR phosphorylation or could result from inhibition of PTP1B-catalyzed dephosphorylation of IRS-1, which has recently been proposed (*58*).

While solutions of the modes of binding for only two of the inhibitors in this series are presented here, they reveal important features that could be exploited for further inhibitor development. One may rationalize the relative K_i values of inhibitors in this series on the basis of the presence or absence of the major binding elements identified by the determined structures of compounds **VI** and **VIII**. The key role played by the main chain carbonyl of the P(−2) residue likely accounts, at least in part, for the superior binding affinity of compound **IV** relative to that of compound **III**, as well as the increased potency of compound **VI** relative to compound **V**. It is also reasonable to assume that the WPD loop is more closed upon binding of compound **V** to PTP1B than it is when the closely related but less potent malonate analogue compound **III** binds. Furthermore, the lipophilic interactions of the P(−1) phenylalanine residue likely account for the improved binding affinity of compound **VIII** relative to compound **III**. Closure of the WPD loop upon binding of compound **VI** is likely an important contributor to its greater potency relative to compound **IV**. Finally, the finding that the PTP1B−inhibitor complexes contain ordered water molecules in the active site suggests that inhibitor modifications to displace the bound water will produce an entropy-driven increase in binding and inhibitor potency (*53*).

In summary, the CCK-derived peptidomimetic inhibitors of PTP1B described here represent a novel template for further development of potent, selective inhibitors, and they exhibit cell activity that further justifies the selection of PTP1B as a therapeutic target.

REFERENCES

1. Kruszynska, Y. T., and Olefsky, J. M. (1996) *J. Invest. Med. 44*, 413−28.
2. Seely, B. L., Staubs, P. A., Reichart, D. R., Berhanu, P., Milarski, K. L., Saltiel, A. R., Kusari, J., and Olefsky, J. M. (1996) *Diabetes 45*, 1379−85.
3. Wang, X. Y., Bergdahl, K., Heijbel, A., Liljebris, C., and Bleasdale, J. E. (2001) *Mol. Cell. Endocrinol. 173*, 109−19.
4. Bandyopadhyay, D., Kusari, A., Kenner, K. A., Liu, F., Chernoff, J., Gustafson, T. A., and Kusari, J. (1997) *J. Biol. Chem. 272*, 1639−45.
5. Ramachandran, C., Aebersold, R., Tonks, N. K., and Pot, D. A. (1992) *Biochemistry 31*, 4232−8.
6. Ahmad, F., Li, P. M., Meyerovitch, J., and Goldstein, B. J. (1995) *J. Biol. Chem. 270*, 20503−8.
7. Kenner, K. A., Anyanwu, E., Olefsky, J. M., and Kusari, J. (1996) *J. Biol. Chem. 271*, 19810−6.
8. Ahmad, F., Azevedo, J. L., Cortright, R., Dohm, G. L., and Goldstein, B. J. (1997) *J. Clin. Invest. 100*, 449−58.
9. Ahmad, F., Considine, R. V., Bauer, T. L., Ohannesian, J. P., Marco, C. C., and Goldstein, B. J. (1997) *Metab. Clin. Exp. 46*, 1140−5.
10. Chen, H., Cong, L. N., Li, Y., Yao, Z. J., Wu, L., Zhang, Z. Y., Burke, T. R., Jr., and Quon, M. J. (1999) *Biochemistry 38*, 384−9.
11. Maegawa, H., Ide, R., Hasegawa, M., Ugi, S., Egawa, K., Iwanishi, M., Kikkawa, R., Shigeta, Y., and Kashiwagi, A. (1995) *J. Biol. Chem. 270*, 7724−30.
12. Elchebly, M., Payette, P., Michaliszyn, E., Cromlish, W., Collins, S., Loy, A. L., Normandin, D., Cheng, A., Himms-Hagen, J., Chan, C. C., Ramachandran, C., Gresser, M. J., Tremblay, M. L., and Kennedy, B. P. (1999) *Science 283*, 1544−8.
13. Burke, T. R., Jr., and Zhang, Z. Y. (1998) *Biopolymers 47*, 225−41.
14. Wrobel, J., Sredy, J., Moxham, C., Dietrich, A., Li, Z., Sawicki, D. R., Seestaller, L., Wu, L., Katz, A., Sullivan, D., Tio, C., and Zhang, Z. Y. (1999) *J. Med. Chem. 42*, 3199−202.
15. Malamas, M. S., Sredy, J., Moxham, C., Katz, A., Xu, W. X., McDevitt, R., Adebayo, F. O., Sawicki, D. R., Seestaller, L., Sullivan, D., and Taylor, J. R. (2000) *J. Med. Chem. 43*, 1293−310.
16. Iversen, L. F., Andersen, H. S., Branner, S., Mortensen, S. B., Peters, G. H., Norris, K., Olsen, O. H., Jeppesen, C. B., Lundt, B. F., Ripka, W., Moller, K. B., and Moller, N. P. H. (2000) *J. Biol. Chem. 275*, 10300−7.
17. Gao, Y., Wu, L., Luo, J. H., Guo, R., Yang, D., Zhang, Z. Y., and Burke, T. R. (2000) *Bioorg. Med. Chem. Lett. 10*, 923−7.
18. Burke, T. R., Yao, Z. J., Zhao, H., Milne, G. W. A., Wu, L., Zhang, Z. Y., and Voigt, J. H. (1998) *Tetrahedron 54*, 9981−94.
19. Yu, L., McGill, A., Ramirez, J., Wang, P. G., and Zhang, P. G. (1995) *Bioorg. Med. Chem. Lett. 5*, 1003−6.
20. Ham, S. W., Park, J. G., Lee, S. J., and Yoo, J. S. (1999) *Bioorg. Med. Chem. Lett. 9*, 185−6.
21. Larsen, S. D., May, P. D., Bleasdale, J. E., Liljebris, C. L., Schostarez, H. J., and Barf, T. (1998) PCT Int. Appl. WO 99/11606, 19990311.
22. Guan, K. L., and Dixon, J. E. (1991) *J. Biol. Chem. 266*, 17026−30.
23. Baykov, A. A., Evtushenko, O. A., and Avaeva, S. M. (1988) *Anal. Biochem. 171*, 266−70.

24. Sizer, K. M., Smith, C. L., Jacob, C. S., Swanson, M. L., and Bleasdale, J. E. (1994) *Mol. Cell. Endocrinol. 102*, 119−29.
25. Koivisto, U. M., Martinez-Valdez, H., Bilan, P. J., Burdett, E., Ramlal, T., and Klip, A. (1991) *J. Biol. Chem. 266*, 2615−21.
26. Tsai, T. D., Shuck, M. E., Thompson, D. P., Bienkowski, M. J., and Lee, K. S. (1995) *Am. J. Physiol. 268*, C1173−8.
27. Songyang, Z., Carraway, K. L., Eck, M. J., Harrison, S. C., Feldman, R. A., Mohammadi, M., Schlessinger, J., Hubbard, S. R., Smith, D. P., Eng, C., Lorenzo, M. J., Ponder, B. A. J., Mayer, B. J., and Cantley, L. C. (1995) *Nature 373*, 536−9.
28. Jia, Z. C., Barford, D., Flint, A. J., and Tonks, N. K. (1995) *Science 268*, 1754−8.
29. Otwinoski, Z., and Minor, W. (1997) *Methods Enzymol. 277*, 307−26.
30. Collaborative Computational Project, Number 4 (1994) *Acta Crystallogr. D50*, 750.
31. Brunger, A. (1993) *X-PLOR*, version 3.1, Yale University Press, New Haven, CT.
32. Murshudov, G. V., Vagin, A. A., and Dodson, E. J. (1997) *Acta Crystallogr. D53*, 240−55.
33. Jones, T. A., Zou, J. Y., Cowan, S. W., and Kjeldgaard, M. (1991) *Acta Crystallogr. A47*, 110−9.
34. Lamzin, V. S., and Wison, K. S. (1997) *Methods Enzymol. 277*, 269−305.
35. Larsen, S. D., et al. (2001) *J. Med. Chem.* (manuscript submitted for publication).
36. Zhang, Z. Y., Wang, Y. A., and Dixon, J. E. (1994) *Proc. Natl. Acad. Sci. U.S.A. 91*, 1624−7.
37. Lee, S. R., Kwon, K. S., Kim, S. R., and Rhee, S. G. (1998) *J. Biol. Chem. 273*, 15366−72.
38. Niculescu, R., Bradford, H. N., Colman, R. W., and Kalf, G. F. (1995) *Chem.-Biol. Interact. 98*, 211−22.
39. Zhang, Z.-Y., Maclean, D., McNamara, D. J., Sawyer, T. K., and Dixon, J. E. (1994) *Biochemistry 33*, 2285−90.
40. Desmarais, S., Jia, Z. C., and Ramachandran, C. (1998) *Arch. Biochem. Biophys. 352*, 225−31.
41. Glover, N. R., and Tracey, A. S. (1999) *J. Am. Chem. Soc. 121*, 3579−89.
42. Kole, H. K., Ye, B., Akamatsu, M., Ford, H., Yan, X., Barford, D., Roller, P. P., and Burke, T. R. (1995) *Biochem. Biophys. Res. Commun. 209*, 817−22.
43. Tonks, N. K., Cicirelli, M. F., Diltz, C. D., Krebs, E. G., and Fischer, E. H. (1990) *Mol. Cell. Biol. 10*, 458−63.
44. Bundgaard, H. (1991) in *A Textbook for Drug Design and Development* (Krogsgaard-Larsen, P., and Bundgaard, H., Eds.) pp 111−91, Harwood Academic Publishers, Chur, Switzerland.
45. Sarmiento, M., Puius, Y. A., Vetter, S. F., Keng, Y.-F., Wu, L., Zhao, Y., Lawrence, D. S., Almo, S. C., and Zhang, Z.-Y. (2000) *Biochemistry 39*, 8171−9.
46. Groves, M. R., Yao, Z.-J., Roller, P. P., Burke, T. T., Jr., and Barford, D. (1998) *Biochemistry 37*, 17773−83.
47. Flocco, M. M., and Mowbray, S. L. (1995) *J. Mol. Biol. 254*, 96−105.
48. Worm, D., Vinten, J., and Beck-Nielsen, H. (1999) *Diabetologia 42*, 1146−7.
49. Goldstein, B. J., Ahmad, F., Ding, W., Li, P. M., and Zhang, W. R. (1998) *Mol. Cell. Biochem. 182*, 91−9.
50. Wallace, A. C., Laskowski, R. A., and Thornton, J. M. (1995) *Protein Eng. 8*, 127−34.
51. Vetter, S. W., Keng, Y. F., Lawrence, D. S., and Zhang, Z. Y. (2000) *J. Biol. Chem. 275*, 2265−8.
52. Glover, N. R., and Tracey, A. S. (1999) *Biochem. Cell Biol. 77*, 469−86.
53. Peters, G. H., Frimurer, T. M., Andersen, J. N., and Olsen, O. H. (2000) *Biophys. J. 78*, 2191−200.
54. Sarmiento, M., Zhao, Y., Gordon, S. J., and Zhang, Z.-Y. (1998) *J. Biol. Chem. 273*, 26368−74.
55. Puius, Y. A., Zhao, Y., Sullivan, M., Lawrence, D. S., Almo, S. C., and Zhang, Z.-Y. (1997) *Proc. Natl. Acad. Sci. U.S.A. 94*, 13420−5.
56. Taing, M., Keng, Y.-F., Shen, K., Wu, L., Lawrence, D. S., and Zhang, Z.-Y. (1999) *Biochemistry 38*, 3793−803.
57. Venable, C. L., Frevert, E. U., Kim, Y.-B., Fischer, B. M., Kamatkar, S., Neel, B. G., and Kahn, B. B. (2000) *J. Biol. Chem. 275*, 18318−26.
58. Goldstein, B. J., Bittner-Kowalczyk, A., White, M. F., and Harbeck, M. (2000) *J. Biol. Chem. 275*, 4283−9.

BI002865V